nature
Vol 278 No 5700 8 March 1979 80p US $2.25

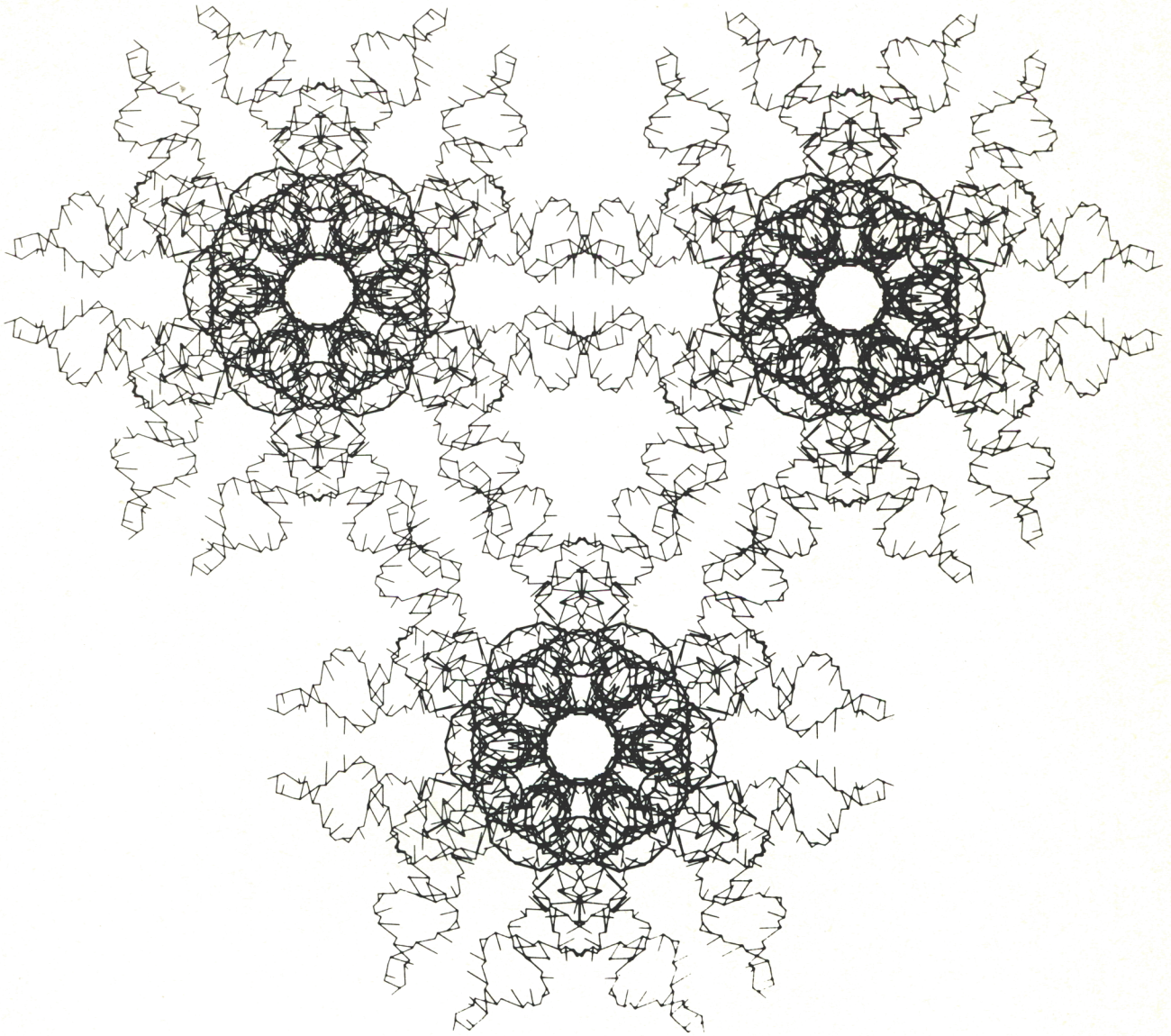

Crystal structure of eukaryotic tRNA

19. Seitz, U. & Seitz, U. *Planta* **97**, 224–229 (1971).
20. Brändle, E. & Zetsche, K. *Planta* **111**, 209–217 (1973).
21. Takebe, I. & Otsuki, Y. *Proc. natn. Acad. Sci. U.S.A.* **64**, 843–848 (1969).
22. Sänger, H. L. & Knight, C. A. *Biochem. biophys. Res. Commun.* **13**, 455–461 (1963).
23. White, J. L. & Murakishi, H. H. *J. Virol.* **21**, 484–492 (1977).
24. Diener, T. O. *Virology* **43**, 75–89 (1971).
25. Sänger, H. L. *Adv. Biosci.* **8**, 103–116 (1972).
26. Semancik, J. S. & Geelen, J. L. M. C. *Nature* **256**, 753–756 (1975).
27. Hadidi, A., Jones, D. M., Gillespie, D. H., Wong-Staal, F. & Diener, T. O. *Proc. natn. Acad. Sci. U.S.A.* **73**, 2453–2457 (1976).
28. Grill, L. K. & Semancik, J. S. *Proc. natn. Acad. Sci. U.S.A.* **75**, 896–900 (1978).
29. Gross, H. J., Domdey, H. & Sänger, H. L. *Nucleic Acids Res.* **4**, 2021–2028 (1977).
30. Langowski, Y., Henco, K., Riesner, D. & Sänger, H. L. *Nucleic Acids Res.* **5**, 1589–1610 (1978).

Crystal structure of a eukaryotic initiator tRNA

OUR understanding of the molecular structure–function relationship in tRNA rests mainly on three types of information. First, on the common sequence patterns which have emerged from careful examination of many primary structures[1–3]; second, a wide variety of spectral and other physical and chemical results must be accounted for by the molecular structure[4–6]; and third, there is the detailed image of the yeast $tRNA^{Phe}$ molecule independently determined and refined from two different—albeit similar—crystal forms[7–10]. It is also clear, however, that the molecular model deduced from the yeast $tRNA^{Phe}$ crystal structure cannot be easily reconciled with all structural requirements for function and is best considered a well-defined and stable canonical form of tRNA which is packed in an unusually well-ordered way in specific crystal lattices. Notwithstanding the enormous value of this canonical form in explaining the basic architectural features of tRNA, it is clearly important to image other crystalline tRNAs; particularly tRNAs that exhibit different functions (such as, initiators) or have significantly different covalent structures (for example, class III tRNAs)[1] or those that crystallise in different solvent conditions. We report here the initial results of the crystal structure determination of a eukaryotic initiator tRNA crystallised from a highly polar aqueous solvent[11,12]. Its architecture is essentially the same as crystalline yeast $tRNA^{Phe}$, except for a small but significant difference in the position of the anticodon arm.

Our interpretation is based on a 4.5 Å electron density map prepared by the method of multiple isomorphous replacement (MIR) and augmented by direct methods[13]. The trace of the sugar–phosphate backbone is further constrained by four heavy-atom markers, each covalently linked to a specific residue and an elaborate network of crystallographic dyads upon which the molecule cannot intrude. The model presented here is based on a low resolution least-squares refinement procedure which assumes that the molecule is organised in four domains corresponding to the arms of the cloverleaf hydrogen-bonding pattern[14].

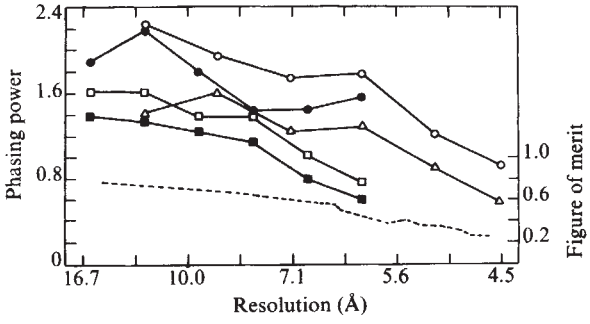

Fig. 1 Phasing power $(\sum|F_H|^2)^{1/2}/(\sum(|F_{PH}^{obs}|-|F_{PH}^{calc}|)^2)^{1/2}$ of five isomorphous derivatives plotted against resolution. They are gadolinium, lightly substituted, precession data (■); gadolinium, heavily substituted, precession data (□); gadolinium, oscillation data (△), pyridyl mercury acetate, precession data (●), and pyridyl mercury acetate, oscillation data (○). Figure of merit (– – –) is determined from MIR phasing[33] and has a mean value of 0.49 for all reflections to 4.5 Å resolution. F_H is the caculated heavy atom structure amplitude; $(|F_{PH}^{obs}|-|F_{PH}^{cal}|)$ is the 'lack of closure' error between observed and calculated isomorphous derivative structure amplitudes.

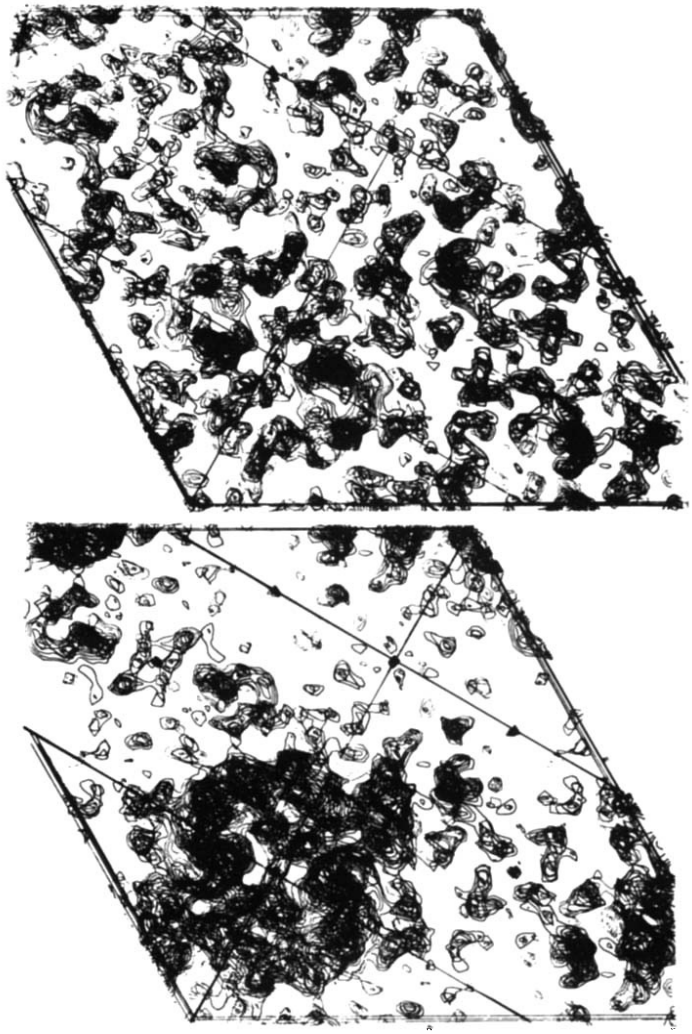

Fig. 2 Comparison of 10 sections of the 4.5 Å map of yeast $tRNA_f^{Met}$ before (above) and after (below) the inclusion of 28 intense low resolution terms determined by matrical phase predictions. Both maps are contoured at the same intervals. Density cleared by this technique was ultimately shown to be noise, while density that was enhanced improved connectivity in the helical stems. Density on the dyad axes diminished.

The crystals have three important chracteristics[15]. (1) They are grown from and stabilised in approximately 2M $(NH_4)_2SO_4$ containing 5 mM Mg^{2+} and 2 mM spermine and no organic solvent. The 2M ammonium ion may alter the structural role attributed to Mg^{2+} and spermine in crystalline yeast $tRNA^{Phe}$ (refs 16–18). (2) Only 17.5% of the crystal volume is occupied by tRNA. Treating the remaining 82.5% as disordered solvent of uniform density was quite helpful in the structure analysis. (3) The crystal is poorly ordered, making accurate data collection very difficult and effectively impossible beyond 4 Å resolution. Data for the parent and three isomorphous heavy atom derivatives were collected intially to 6 Å by procession photography and extended to 4.0 Å by oscillation photographs in which a single crystal was devoted to each of ~30 overlapping 2.5° or 2° sectors. Figure 1 shows that there is useful phasing power in the best derivative to about 4.5 Å resolution. Schevitz *et al.*[15] presented a 6 Å analysis of the yeast $tRNA_f^{Met}$ crystal structure. Despite two heavy atom markers at iodine $^5C_{73}$ (5-bonding onto cytosine at residue 73) and osmium $^{5,6}C_{38}$ the electron density could not be convincingly interpreted in terms of the molecular backbone. Even when the data for the parent structure and MIR

0028-0836/79/0278—0188$01.00
© Macmillan Journals Ltd 1979

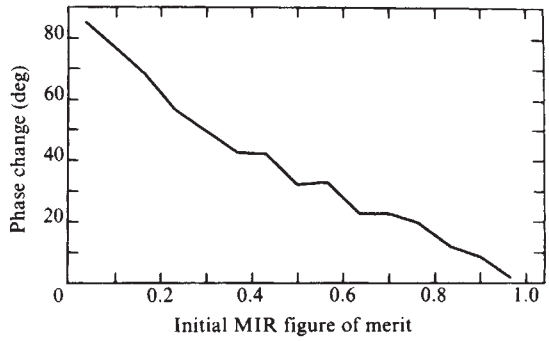

Fig. 3 Final phase change in degrees resulting from direct methods (see text) as a function of the original figure of merit determined by conventional MIR phasing. Phase information from both sources was merged by multiplying together their respective phase probability curves after each cycle of combined solvent levelling and density modification. Note that those reflections predicted to have a high reliability by MIR phasing (figure of merit near 1.0) remained closely tethered to their MIR phase while those with a low MIR reliability (figure of merit near 0) tend to be more easily shifted toward phases calculated by direct methods.

phases were extended to 4.5 Å resolution and a third heavy atom marker at iodine $^5U_8$ was used the map was still too 'noisy' to interpret confidently.

One particularly vexing deficiency in the MIR map was the inability to define the exact molecular boundary with confidence. As over 80% of the unit cell volume was solvent this structure was particularly amenable to phase improvement by solvent levelling if the molecular boundary could be accurately established[19,20]. The boundary was established by phasing the previously omitted very intense inner reflections ($d > 14$ Å). In the effort to secure high resolution data by extensively irradiating each crystal, these strong reflections were overexposed and far exceeded the dynamic range of even the most weakly exposed film. Even if relatively accurate amplitudes had been obtained for the parent and derivatives it is likely that the heavy atom contribution would not have been strong enough to provide accurate difference amplitudes to phase the very strongest of these reflections. To circumvent this problem the inner core of intense parent intensities was accurately remeasured and the phases of 28 of the very strongest reflections were determined by applying matricial methods to the amplitudes and MIR phases of 107 known reflections. The technique is similar to that used by Podjarny *et al.* to extend the phases of triclinic lysome[21] and yeast $tRNA^{Phe}$ (ref. 22) to a higher resolution than the starting phase set. Here the procedure was used to extend phases to a lower resolution than the MIR phase set. The details of this work will be published elsewhere[13]; however, it is evident from Fig. 2 that there was substantial enhancement of the contrast between the molecule and the solvent. The improved map enabled us to confidently define 65% of the unit cell as solvent. New phases were calculated from a map in which the noise in the 'solvent' was levelled to a uniform average value and negative regions in the molecule attenuated[23,24]. These phases were merged with

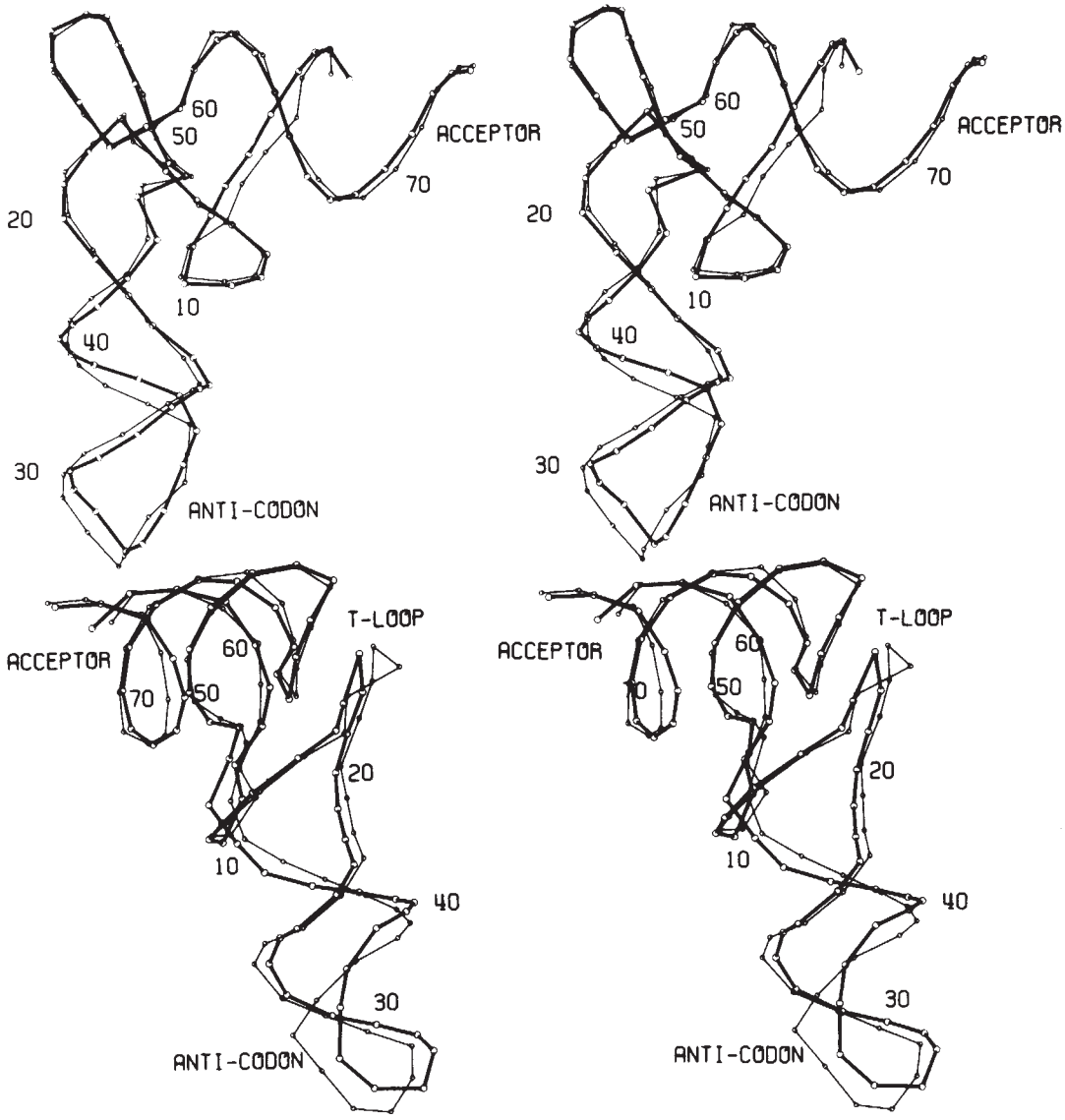

Fig. 4 Comparison of the yeast $tRNA_f^{Met}$ (heavy line) and yeast $tRNA^{Phe}$ (light line) structures in two stereo views. The phosphate backbone is shown with every tenth phosphate residue of yeast $tRNA_f^{Met}$ numbered.

©1979 Nature Publishing Group

MIR phases and the 'density modification' procedure repeated for three cycles. Figure 3 shows that the phase improvement effected by density modification was most apparent for those reflections whose MIR phase was, in general, least accurate.

Four residues have been reacted stoichiometrically with covalently bonded heavy atoms. The heavy-atom markers were nicely distributed along the molecular backbone and provided a clear guide to the interpretation. (1) Iodine $^{5}C_{73}$: the third residue from the 3′ terminus was labelled with iodine either by enzymatically rebuilding the 3′ terminus with iodine ^{5}CTP and nucleotidyl transferase[25] or by directly iodinating the crystals[26]. (2) iodine $^{5}C_{74}$: direct iodination also labels C_{74} which shows a small peak that cannot be refined, presumably because of disorder. (3) Iodine $^{5}U_{8}$: produced by direct iodination of the crystal[26]. (4) Osmium $^{5,6}C_{38}$: direct reaction of the crystals with Os(VI) and pyridine[27] forming a 5,6-bispyridyl osmate diester[28,29] with C_{38} (ref. 30).

Initially we interpreted the map with a conventional optical comparator and skeletal models, but it was found more convenient to use computerised 'static' molecular graphics[31] to search for significantly different orientations of the stable helical substructures operating within the constraints imposed by the heavy atom markers and the crystallographic dyad axes upon which the model could not intrude. Subsequently, a residue-by-residue computerised fit of the entire model to the map was attempted in 'real time' at the Computer Graphics Laboratory at the University of North Carolina and this allowed us to rule out additional alternatives; however, we found the map was not sufficiently well resolved to impose a correspondence between phosphate, ribose and base moieties in the model and the peaks in the electron density.

The coordinates of the optimal fit were used as guides to position a $tRNA^{Phe}$ model[10] in the $P6_422$ unit cell. The root-mean-square deviation between the guide points and the $tRNA^{Phe}$ model coordinates was 5.4 Å. This model was divided into four rigid groups corresponding to the helical arms and refined against observed intensities using a least squares procedure (CORELS) of Sussman *et al.*[32] that 'restrained' the helical arms to remain within reasonable bonding distance of each other. The refinement was started at 12.5 Å and carried to 6 Å. The final crystallographic *R* factor between calculated and observed data to 6 Å was 42.3%; to 12 Å, 33%. These values indicate an essentially correct interpretation of a macromolecular crystal structure.

The molecular structure is shown in Fig. 4 contrasted with that of yeast $tRNA^{Phe}$. Except for a small region near the anticodon stem, the model accounts for virtually all the electron density in terms of a dominant sugar phosphate backbone. At this stage of the analysis the molecular architecture is generally similar to that of yeast $tRNA^{Phe}$.

The position of the anticodon arm in the crystal structure of yeast $tRNA_f^{Met}$ differs significantly from the crystal structure of yeast $tRNA^{Phe}$ (Fig. 4). Moreover, the refinement parameters show that although the anticodon arm converges to the position shown in Figure 4, it is the most poorly localised segment of the crystal structure. These observations suggest that the orientation of the anticodon arm is not rigidly fixed and the union of the D and anticodon stems may, as suggested previously[18,34], serve as a hinge point to allow alterations in the orientation of the anticodon during functional adjustments of the structure. Except for the possible stacking of a non Watson–Crick pair $m_2^2G_{26}$ and A_{44}, no stabilising tertiary interaction can be invoked to ensure a particular orientation of the anticodon arm.

The molecules are packed with all 12 of the acceptor-T helices in the unit cell clustered around the 6_4 axis at an angle of approximately 20°. Pairs of neighbouring molecules that have opposing acceptor stems stack upon one another roughly in helical register. This explains the intense continuous helical diffraction pattern along c^* observed at approximately 3 Å resolution, well beyond the lattice transform[15].

The anticodon arms project out roughly perpendicular to the 6_4 axes and contact neighbouring molecules at their anticodon loop and the base of the D-stem. Thus many of the stabilising interactions involve the anticodon arm, which we believe to be extended on a flexible hinge. The fact that the lattice is connected through these hinged anticodon arms may be the reason that this (and possibly many other) tRNA crystals, although readily grown, are poorly ordered. The situation is reminiscent of the characteristically poorly ordered crystalline immunoglobulins[35]—another macromolecule where flexibly hinged domains may be necessary for function.

R.W.S. was a fellow of the American Cancer Society, Damon Runyon/Walter Winchell Foundation, and USPHS. A.D.P. is a fellow of the Damon Runyon/Walter Winchell Foundation; NK was a fellow of USPHS, and J.J.H. was a USPHS trainee. This work was supported by grants from the NSF, USPHS, and American Cancer Society. The Weizmann Institute Computer Center provided computer facilities.

Note added in proof: Refinement with a more flexible model has reduced the crystallographic R-factor to 25% for all data to 4.0 Å resolution. Difference maps are clean and tertiary structural interactions are seen which can be correlated to those in crystalline yeast $tRNA^{Phe}$.

RICHARD W. SCHEVITZ
ALBERTO D. PODJARNY*
N. KRISHNAMACHARI†
JOHN J. HUGHES‡
PAUL B. SIGLER

Department of Biophysics and Theoretical Biology, University of Chicago, Chicago, Illinois 60637

JOEL L. SUSSMAN

Department of Structural Chemistry, Weizmann Institute of Science, Rehovot, Israel

Received 27 November; accepted 18 December 1978.

*Permanent address: Laboratorio de Rayos-X, Departamento de Fisica UNLP, CC 67 La Plata 1900, Argentina.
†Present address: Computation Center, University of Chicago, Chicago, Illinois 60637.
‡Present address: Whitlow Corporation, Englewood Cliffs, New Jersey, 07632.

1. Levitt, M. *Nature* **224,** 759 (1969).
2. Barrell, B. G. & Clark, B. F. C. *Handbook of Nucleic Acid Sequences* (Joynson-Bruvvers, Oxford, 1974).
3. Sprinzl, M., Grüter, F. & Gauss, D. H. *Nucleic Acids Res.* Special Supplement r15 (1978).
4. Sigler, P. B. *A. Rev. Biophys. Bioengng* **4,** 477 (1975).
5. Kim, S.-H. *Prog. Nucleic Acid Res. molec. Biol.* **17,** 181 (1976).
6. Rich, A. & RajBhandary, V. L. *A. Rev. Biochem.* **45,** 805 (1976).
7. Quigley, G. J. *et al. Proc. natn. Acad. Sci. U.S.A.* **72,** 4866 (1975).
8. Jack, A., Ladner, J. E. & Klug, A. *J. molec. Biol.* **108,** 619 (1976).
9. Stout, C. D. *et al. Nucleic Acids Res.* **3,** 1111 (1976).
10. Sussman, J. L., Holbrook, S. R., Warrant, R. W., Church, G. M. & Kim, S.-H. *J. molec. Biol.* **123,** 607 (1978).
11. Young, J. D. *et al. Science* **166,** 1527 (1969).
12. Johnson, C. D., Adolph, R., Rosa, J. J., Hall, M. D. & Sigler, P. B. *Nature* **226,** 1246 (1970).
13. Podjarny, A. D., Schevitz, R. W., Hughes, J., Zwick, M. & Sigler, P. B. (in preparation).
14. Holley, R. W. *et al. Science* **147,** 1462 (1965).
15. Schevitz, R. W. *et al.* in *Structure and Conformation of Nucleic Acids and Protein-Nucleic Acid Interactions* (eds Sundaralingam, M. & Rao, S. T.) 85 (University Park Press, Baltimore, 1975).
16. Jack, A., Ladner, J. E., Rhodes, D., Brown, R. S. & Klug, A. *J. molec. Biol.* **111,** 315 (1977).
17. Quigley, G. J., Teeter, M. M. & Rich, A. *Proc. natn. Acad. Sci. U.S.A.* **75,** 64 (1978).
18. Holbrook, S. R., Sussman, J. L., Warrant, R. W. & Kim, S.-H. *J. molec. Biol.* **123,** 631 (1978).
19. Bricogne, G. *Acta Crystallogr.* A **32,** 832 (1976).
20. Hendrickson, W. A. in *Current Trends in Biomolecular Structure* (ed. Srinivasan, R.) (Pergamon, Oxford, in the press).
21. Podjarny, A. D., Yonath, A. & Traub, W. *Acta Crystallogr.* A **32,** 281 (1976).
22. Podjarny, A. D. & Yonath, A. *Acta Crystallogr.* A **33,** 655 (1977).
23. Collins, D. M. *et al. Science* **190,** 1047 (1975).
24. Barrett, A. N. & Zwick, M. *Acta Crystallogr.* **27,** 6 (1971).
25. Pasek, M., Venkatappa, M. P. & Sigler, P. B. *Biochemistry* **12,** 4834 (1973).
26. Tropp, J. S. & Sigler, P. B. (in preparation).
27. Schevitz, R. W. *et al. Science* **177,** 429 (1972).
28. Neidle, S. & Stuart, D. I. *Biochim. biophys. Acta* **418,** 226 (1976).
29. Kistenmacher, T. J., Marzilli, L. G. & Rossi, M. *Bioinorg. Chem.* **6,** 347 (1976).
30. Rosa, J. J. & Sigler, P. B. *Biochemistry* **13,** 5102 (1974).
31. Podjarny, A. D. thesis, Weizmann Institute of Science, Rehovot (1976).
32. Sussman, J. L., Holbrook, S. R., Church, G. M. & Kim, S.-H. *Acta Crystallogr.* A **33,** 243 (1977).
33. Blow, D. M. & Crick, F. H. C. *Acta Crystallogr.* **12,** 794 (1959).
34. Robertus, J. D. *et al. Nature* **250,** 546 (1974).
35. Silverton, E. W., Navia, M. A. & Davies, D. R. *Proc. natn. Acad. Sci. U.S.A.* **74,** 5140 (1977).

©1979 Nature Publishing Group